Electron spin dynamics in Ce^{3+} : YAG crystals: Hyperfine interaction of 4*f* and 5*d* electrons

P. Liang,[1] Z. Wu,[1] Y. Y. Zhang,[1] R. R. Hu,[1] T. Q. Jia,[1] Y. Yang,[1] S. A. Zhang,[1] Z. R. Sun,[1] and D. H. Feng[1,2,*]

[1]*State Key Laboratory of Precision Spectroscopy, East China Normal University, Shanghai 200062, China*

[2]*Collaborative Innovation Center of Extreme Optics, Shanxi University, Taiyuan, Shanxi 030006, China*

(Received 31 August 2018; revised manuscript received 14 November 2018; published 16 January 2019)

The electron spin dynamics of Ce^{3+} ions in YAG crystals is studied by time-resolved photoluminescence spectroscopy with an alternating left and right circularly polarized continuous-wave laser modulation technique. The electron spin relaxation due to hyperfine interaction with randomly oriented nuclear spins can be efficiently suppressed by a weak external longitudinal magnetic field. The suppression of the hyperfine-induced spin relaxation makes the electron spin polarization increase from 0.001 to 0.016 for the lowest $4f$ state, and from 0.08 to 0.32 for the lowest $5d$ state. The suppression magnetic fields for the $4f$ electrons are several times weaker than that for the $5d$ electrons, dependent on the crystal orientation. The dispersion of the local hyperfine field distribution ΔB is isotropic and equal to 4.0 mT for the $5d$ electrons, and anisotropic for the $4f$ electrons with $\Delta B_{[001]} = 0.8$ mT, $\Delta B_{[110]} = 1.1$ mT, $\Delta B_{[1\bar{1}0]} = 2.4$ mT. The hyperfine coupling strength for the $4f$ electrons is ~4 times weaker than that for the $5d$ electrons.

DOI: 10.1103/PhysRevB.99.024308

I. INTRODUCTION

The electron spin states have initiated extensive research for their prospective application in quantum information processing [1,2]. Dopants in solids and semiconductor quantum dots are often-studied materials because of their spatially localized electron wave function, which helps to maintain long spin lifetimes [3–5]. At low temperature and in the absence of or weak magnetic field, electron spin relaxation in these systems is dominated by the electron-nuclear hyperfine interaction. Previous studies on hyperfine interaction usually viewed the electron g tensor as isotropic [6–9]. In practical systems, the electron g tensor could have strong anisotropy [10,11].

Rare-earth cerium-doped garnet crystals are well-known scintillators with high performance and high luminous efficiency [12,13]. In recent years, optically oriented electron spin states of Ce^{3+} ions in yttrium aluminum garnet (YAG, $Y_3Al_5O_{12}$) crystals have attracted much interest [14–17]. Optical pumping can initialize the spin of both the $4f$ ground and $5d$ excited electrons of Ce^{3+} ions. The $5d$ electron spin is thermally robust and can be detected up to room temperature. The $5d$ electron g tensor is quasi-isotropic with a value of ~2.0, as measured by time-resolved pump-probe Faraday rotation spectroscopy [17]. In contrast, the $4f$ electron spin is observed only at low temperature [16] and the g tensor is strongly anisotropic [11,16,18]. It has been revealed that electron-nuclear hyperfine interaction dominates the electron spin relaxation both in the $4f$ and $5d$ states at weak magnetic fields [14–17]. The nuclear hyperfine field is mainly provided by neighboring ^{27}Al nuclei (spin $I = 5/2$, 100% natural abundance) due to the fact that all the cerium nuclei have zero nuclear spin. For the $4f$ ground electrons of Ce^{3+} ions, the transferred hyperfine interaction with the nearest Al^{3+} ions has been confirmed by pulsed-electron nuclear double resonance (ENDOR) techniques [19,20]. For different shell electrons of the $4f$ and $5d$ states, however, it is unclear whether or not the properties of hyperfine coupling are different, such as hyperfine coupling strength and the dispersion of the local hyperfine field distribution ΔB.

The often-used optical techniques for detecting electron spin dynamics include time-resolved photoluminescence and pump-probe measurements with pulse lasers. Time-resolved photoluminescence measurements under instantaneous pumping typically detect the electron spin dynamics of the excited states. The pump-probe technique, including time-resolved Faraday and Kerr rotation spectroscopy, is sensitive to both the ground- and excited-state electron spins. Pump-probe measurements usually make it hard to directly separate the longitudinal electron spin signals between the ground and excited states. Furthermore, pump-probe measurements are difficult to quantify the spin polarization degree of ensemble electrons. In this work, we study the hyperfine interaction in parallel for the $4f$ and $5d$ electrons of Ce^{3+} ions and the influence of longitudinal magnetic fields. Under an alternating continuous-wave σ^+/σ^- circular polarization laser excitation, electron spin dynamics can be directly evaluated from the photoluminescence (PL) transients [21,22]. Via this technique, the $4f$ and $5d$ electron spin signal can be separately identified in one measurement, from which the information of the electron spin polarization degree and spin lifetime can be extracted. A weak external longitudinal magnetic field can efficiently suppress electron spin relaxations due to the hyperfine interaction with randomly oriented nuclear spins. The value of the dispersion of the local hyperfine field distribution ΔB is obtained for both the $5d$ and $4f$ electrons. ΔB is anisotropic for the $4f$ electrons and isotropic for the $5d$ electrons.

*dhfeng@phy.ecnu.edu.cn

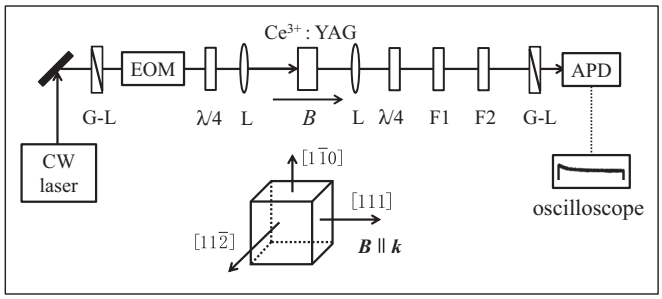

FIG. 1. Experimental setup for electron spin dynamics measurements. The sample Ce^{3+}: YAG crystal is [111] oriented. Light vector $\boldsymbol{k}$ || magnetic field $\boldsymbol{B}$ || [111]. EOM: electro-optical modulator; G-L: Glan-laser polarizer. F1-500 nm long wave pass filter; F2-532 nm band pass filter with bandwidth 10 nm. APD: avalanche photodiode.

II. EXPERIMENTAL METHOD

The sample is a [111]-oriented Ce-doped YAG crystal with a thickness of 0.5 mm and cerium content of 0.2 at.% (Hangzhou Shalom Electro-optics Technology Co., Ltd.). The crystal is mounted in a closed-cycle cryostat, with the sample temperature set at ~5 K. The cryostat is placed in an electromagnet with removable iron poles. The setup for electron spin dynamics measurements is shown in Fig. 1. The excitation laser is a low-noise diode-pumped solid-state continuous-wave laser of 473 nm with linear polarization. An electro-optical modulator and a $\lambda/4$ wave plate are used to alternatingly modulate the laser between σ^+ and σ^- circular polarization. The laser wave vector is parallel to the [111] crystal orientation and the magnetic field **B** (the Faraday configuration). The PL circular polarization is distinguished by a $\lambda/4$ wave plate and a Glan-laser polarization analyzer. After blocking the excitation light by a long-wave pass filter of 500 nm, the PL signal is detected in σ^+ polarization mode by an avalanche photodiode (APD) together with a digital oscilloscope (OSC, LeCroy Wavepro 760Zi) for time-resolved PL measurements.

III. RESULTS AND DISCUSSIONS

As is known, the $4f$ shell of Ce^{3+} ions has only one unpaired electron, which can be optically excited into the $5d$ state [17]. The spin-orbit coupling splits the $4f$ state into $^2F_{5/2}$ and $^2F_{7/2}$ manifolds and the $5d$ state into $^2D_{3/2}$ and $^2D_{5/2}$ manifolds. The crystal field splits the $4f$ and $5d$ states further into 7 and 5 Kramer's doublets, respectively. The Kramer's doublets are further split into spin-up and spin-down states by external magnetic fields.

Figure 2 shows the steady-state PL spectra of Ce^{3+} : YAG crystals under either σ^+ or σ^- circular polarization excitation at 5 K, with the detection fixed in σ^+ mode. There are typically two fluorescence peaks centered at 534 and 588 nm. The 534 nm band corresponds to the transition from the lowest $5d$ state into the lowest $^2F_{5/2}$ state. The 588 nm band is dominated by the transition from the lowest $5d$ state into the $^2F_{7/2}$ manifolds. As shown in Fig. 2, the 534 nm PL band is circularly polarized with the same polarization as the excitation laser, while the 588 nm band has opposite circular polarization to the excitation laser. When the external

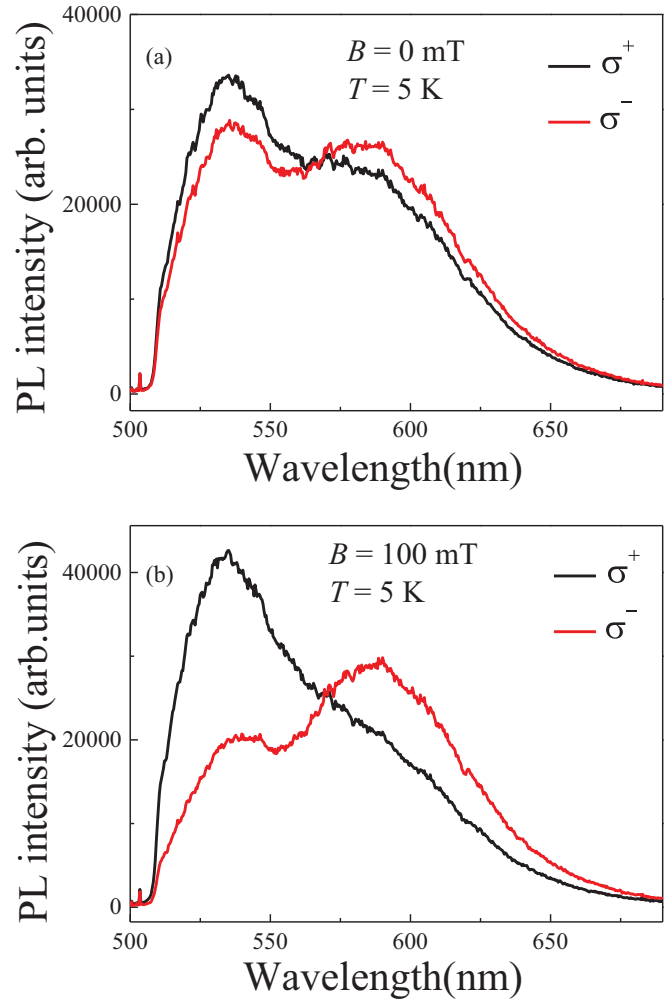

FIG. 2. PL spectra of Ce^{3+} : YAG crystals under σ^+ and σ^- circular polarization excitation at low temperature $T = 5$ K. The longitudinal magnetic field (a) $B = 0$ mT and (b) $B = 100$ mT. The excitation wavelength is 473 nm. The signal detection is fixed in the σ^+ polarization mode.

longitudinal magnetic field is changed from zero to 100 mT, the σ^+ circular polarization degree increases from 8% to 36% for the 534 nm peak; meanwhile, the σ^- circular polarization degree increases from 7% to 15% for the 588 nm peak.

In the time-resolved PL measurements, the detection window is set from 528 to 537 nm with a 532 nm band pass filter of 10 nm bandwidth. Figure 3 shows the time-resolved PL spectra of Ce^{3+} : YAG crystals under the excitation of periodic circular polarization switching at zero and 30 mT magnetic field and low temperature of 5 K. At both zero and 30 mT, the PL signal under copolarized excitation-detection mode is larger than that for counterpolarization. At $B =$ 30 mT, the PL signal weakens gradually to a steady state under copolarized excitation-detection mode. In contrast, the amplitude of the PL gradual change is much less at $B = 0$ mT. The intensity difference between the co- and counterpolarization mode for $B = 0$ mT is evidently smaller than that for 30 mT.

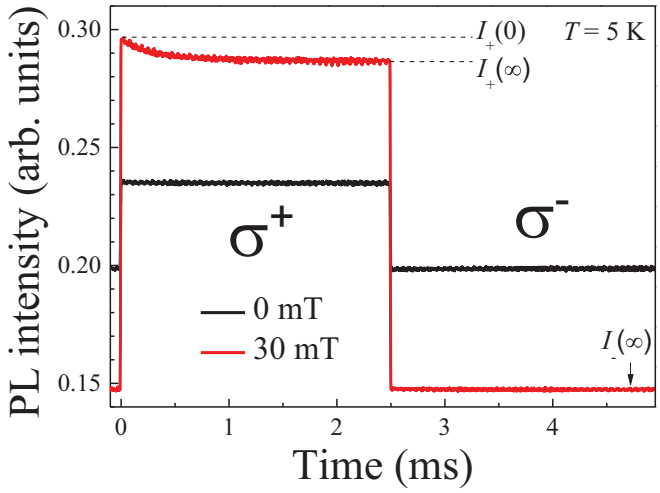

FIG. 3. PL transients under periodic circularly polarized switching excitation at zero and weak external magnetic field $B = 30$ mT for low temperature $T = 5$ K; signal detection is always in the σ^+ polarization mode.

In order to quantitatively understand the PL transients in Fig. 3, now we discuss the optical excitation and decay processes and establish the corresponding rate equations. Figure 4(a) shows the optical transitions of Ce^{3+} ions in YAG crystals under circularly polarized light excitation. The excitation laser wavelength 473 nm is within the phonon-assisted absorption band labeled $5d(1)^{ph}$ [17]. $4f(1)$ and $5d(1)$ are the lowest-energy level of the $4f$ and $5d$ states, respectively. For the sake of simplification, $4f(n)$ includes all the other $4f$ states except for $4f(1)$. Circular polarization selective excitation generates electron spin polarization both in the $4f(1)$ and $5d(1)$ states. Let us say that σ^+ circularly polarized light selectively excites spin-down electrons in the $4f(1)$ state into the spin-up $5d(1)^{ph}$ state. After excitation, the spin-up electrons in $5d(1)^{ph}$ can directly relax to the spin-up $5d(1)$ state or first spin flip to the spin-down $5d(1)^{ph}$ state and then relax to the spin-down $5d(1)$ state. Similarly, the spin-up electrons in $5d(1)$ can directly emit σ^+ photons back to the spin-down $4f(1)$ state or first spin flip to the spin-down $5d(1)$ state and then emit σ^- photons to the spin-up $4f(1)$ state. In this way, a part of the spin-down electrons in $4f(1)$ will be transferred to the arm of the spin-up $4f(1)$ state and a net spin-up polarization of the $4f(1)$ electrons is built up. In the same way, the transition from $5d(1)$ to $4f(n)$ also drives the spin-down $4f(1)$ electrons to the other arm. Continuous excitation makes spin polarization of the $4f(1)$ electrons larger and larger, and finally to a steady state as shown in Fig. 4(b). Now, switching from σ^+ to σ^- excitation starts up an opposite scenario with establishing a net spin-down $4f(1)$ electron. The nonequilibrium between the two arms of the $5d(1)$ state directly leads to electron spin polarization and circularly polarized emission. Selective excitation transfers the electron from one $4f(1)$ arm to the other. The decreased electron population in the corresponding arm leads to a weakened absorption, and thus the PL signal decreases, as shown in Fig. 3. Tracking the associated emission transients thus directly reveals the electron spin evolution.

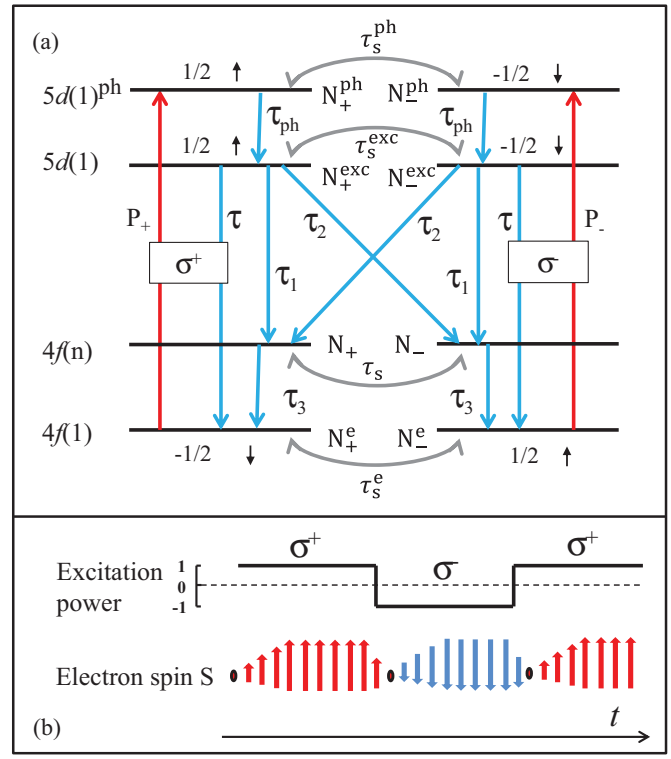

FIG. 4. (a) Optical transitions of Ce^{3+} ions in YAG crystals under circularly polarized light excitation. ↑, ↓ : electron spin; τ_{ph} : the electron lifetime in the $5d(1)^{ph}$ state; τ, τ_1, and τ_2 : the radiative lifetimes of the $5d(1)$ state; τ_3 : the time of the transition from $4f(n)$ to $4f(1)$; τ_s^{ph}, τ_s^{exc}, τ_s, and τ_s^e : spin-flip time of electrons in the $5d(1)^{ph}$, $5d(1)$, $4f(n)$, and $4f(1)$, respectively; $P_\pm$: optical pumping rates. (b) Schematic of electron spin excitation and evolution dynamics.

The corresponding rate equations in Fig. 4(a) are

$$\dot{N}_\pm^e = -P_\pm N_\pm^e + \frac{1}{\tau}N_\pm^{exc} + \frac{1}{\tau_3}N_\pm \mp \frac{1}{2\tau_s^e}(N_+^e - N_-^e), \quad (1)$$

$$\dot{N}_\pm = \frac{1}{\tau_1}N_\pm^{exc} + \frac{1}{\tau_2}N_\mp^{exc} - \frac{1}{\tau_3}N_\pm \mp \frac{1}{2\tau_s}(N_+ - N_-), \quad (2)$$

$$\dot{N}_\pm^{exc} = -\left(\frac{1}{\tau} + \frac{1}{\tau_1} + \frac{1}{\tau_2}\right)N_\pm^{exc} + \frac{1}{\tau_{ph}}N_\pm^{ph} \mp \frac{1}{2\tau_s^{exc}}(N_+^{exc} - N_-^{exc}), \quad (3)$$

$$\dot{N}_\pm^{ph} = P_\pm N_\pm^e - \frac{1}{\tau_{ph}}N_\pm^{ph} \mp \frac{1}{2\tau_s^{ph}}(N_+^{ph} - N_-^{ph}), \quad (4)$$

and the unity condition

$$N_+^e + N_-^e + N_+ + N_- + N_+^{exc} + N_-^{exc} + N_+^{ph} + N_-^{ph} = 1, \quad (5)$$

where $N_\pm^e$, $N_\pm$, $N_\pm^{exc}$, and $N_\pm^{ph}$ represent the electron populations in the two arms of the $4f(1)$, $4f(n)$, $5d(1)$, and $5d(1)^{ph}$ states, respectively. τ_{ph} is the electron lifetime in the $5d(1)^{ph}$ state. τ, τ_1, and τ_2 are the radiative lifetimes of the $5d(1)$ state. τ_3 is the transition time from $4f(n)$ to $4f(1)$. τ_s^{ph}, τ_s^{exc}, τ_s, and τ_s^e are the spin-flip times of electrons at the state of $5d(1)^{ph}$, $5d(1)$, $4f(n)$, and $4f(1)$, respectively. $P_\pm$ are the optical pumping rates, where $P_+ = P_0$, $P_- = 0$ for σ^+ excitation and $P_- = P_0$, $P_+ = 0$ for σ^- excitation.

The intensity of emission from the crystal is proportional to the electron population in the excited state, i.e., $I_+ \propto N_+^{\rm exc}/\tau$ and $I_- \propto N_-^{\rm exc}/\tau$. Solving the rate equations (1)–(4), the PL intensity under alternating σ^+ and σ^- excitation depends on the steady-state electron spin polarization of the $4f(1)$ state $\rho_{\rm s}^{\rm g}$ and can be expressed by

$$I_+(t) \propto \frac{P_0}{4}\left(\frac{2}{\frac{\tau}{\tau_1}+\frac{\tau}{\tau_2}+1}-Q\right)\left(1-\rho_{\rm s}^{\rm g}+2\rho_{\rm s}^{\rm g}e^{-\frac{t}{\tau_R}}\right), \quad (6)$$

$$I_-(t) \propto \frac{P_0}{4}Q\left(1-\rho_{\rm s}^{\rm g}+2\rho_{\rm s}^{\rm g}e^{-\frac{t}{\tau_R}}\right), \quad (7)$$

$$I_+(0) \propto \frac{P_0}{4}\left(\frac{2}{\frac{\tau}{\tau_1}+\frac{\tau}{\tau_2}+1}-Q\right)\left(1+\rho_{\rm s}^{\rm g}\right), \quad (8)$$

$$I_+(\infty) \propto \frac{P_0}{4}\left(\frac{2}{\frac{\tau}{\tau_1}+\frac{\tau}{\tau_2}+1}-Q\right)\left(1-\rho_{\rm s}^{\rm g}\right), \quad (9)$$

$$I_-(\infty) \propto \frac{P_0}{4}Q\left(1-\rho_{\rm s}^{\rm g}\right), \quad (10)$$

where the parameter Q includes all lifetimes in the optically excited states,

$$Q=\left[\left(\frac{\tau_{\rm s}^{\rm exc}}{\tau_1}+\frac{\tau_{\rm s}^{\rm exc}}{\tau_2}+\frac{\tau_{\rm s}^{\rm exc}}{\tau}\right)^{-1}+\left(1+\frac{\tau_{\rm s}^{\rm ph}}{\tau_{\rm ph}}\right)^{-1}\right]\Big/\left(\frac{\tau}{\tau_1}+\frac{\tau}{\tau_2}+\frac{\tau}{\tau_{\rm s}^{\rm exc}}+1\right), \quad (11)$$

$$\frac{1}{\tau_R}=\frac{1}{2}Q_S P_0+\frac{1}{\tau_{\rm s}^{e}}, \quad (12)$$

and

$$Q_S=1-\frac{[\tau_1\tau_2(\tau_3+\tau_s)+\tau\tau_{\rm s}(\tau_2-\tau_1)]\tau_{\rm s}^{\rm exc}\tau_{\rm s}^{\rm ph}}{(\tau_3+\tau_{\rm s})\left(\tau_{\rm ph}+\tau_{\rm s}^{\rm ph}\right)\left(\tau_1\tau\tau_{\rm s}^{\rm exc}+\tau_2\tau\tau_{\rm s}^{\rm exc}+\tau_1\tau_2\tau_{\rm s}^{\rm exc}+\tau_1\tau_2\tau\right)}. \quad (13)$$

$I_+(0)$ and $I_+(\infty)$ stand for the PL intensities under σ^+ excitation at $t=0$ and $t=\infty$, respectively, and $I_-(\infty)$ represents the PL intensity under σ^- excitation at $t=\infty$. From Eqs. (8) and (9), we can obtain

$$\rho_{\rm s}^{\rm g}=[I_+(0)-I_+(\infty)]/[I_+(0)+I_+(\infty)]. \quad (14)$$

The electron spin polarization of the $5d(1)$ state $\rho_{\rm s}^{\rm exc}$ equals the PL circular polarization. From Eqs. (9) and (10), $\rho_{\rm s}^{\rm exc}$ is described by

$$\begin{aligned}\rho_{\rm s}^{\rm exc}&=[I_+(\infty)-I_-(\infty)]/[I_+(\infty)+I_-(\infty)]\\&=\left\{\left(1+\tau_{\rm ph}/\tau_{\rm s}^{\rm ph}\right)\left[1+\left(1/\tau_{\rm s}^{\rm exc}\right)/(1/\tau+1/\tau_1+1/\tau_2)\right]\right\}^{-1}.\end{aligned} \quad (15)$$

As expected, $\rho_{\rm s}^{\rm exc}$ depends on the ratio of the spin relaxation rate $1/\tau_{\rm s}^{\rm exc}$ and radiative rate $1/\tau+1/\tau_1+1/\tau_2$, and the ratio of the spin relaxation rate $1/\tau_{\rm s}^{\rm ph}$ and relaxation rate $1/\tau_{\rm ph}$.

From the experimental data in Fig. 3, we can obtain the steady-state spin polarization of the $4f(1)$ state $\rho_{\rm s}^{\rm g}$ and the $5d(1)$ state $\rho_{\rm s}^{\rm exc}$. Figures 5(a) and 5(b) show $\rho_{\rm s}^{\rm g}$ and $\rho_{\rm s}^{\rm exc}$ as a function of longitudinal magnetic field B. As is shown in Fig. 5(a), the spin polarization of the $4f(1)$ state increases rapidly from 0.001 to 0.016 when the magnetic field is increased from zero to 5 mT. When $B>5$ mT, $\rho_{\rm s}^{\rm g}$ levels off. The spin polarization of the $5d(1)$ state $\rho_{\rm s}^{\rm exc}$ has similar magnetic field dependence, but just needs a larger magnetic field of 20 mT for leveling off. $\rho_{\rm s}^{\rm exc}$ increases from 0.08 to 0.32 with application of the magnetic field. The magnetic field dependences of both $\rho_{\rm s}^{\rm g}$ and $\rho_{\rm s}^{\rm exc}$ agree well with the expectation for the electron spin dynamics dominated by the hyperfine coupling mechanism. As demonstrated in Ref. [6], for an ensemble electron spin polarization that is instantaneously created, the electron spin polarization decays to a steady-state value $R_\parallel(\infty)$ of 1/3 of its initial polarization and 2/3 relaxes fast due to electron-nuclei hyperfine coupling in zero external magnetic field. Increasing longitudinal magnetic fields makes the fast component less and the value of $R_\parallel(\infty)$ tends to 1. The magnetic field dependence of $R_\parallel(\infty)$ can be expressed by [6]

$$R_\parallel(\infty)=1-\frac{1}{\sqrt{\pi}}\int_{-\infty}^{\infty}dz\int_0^{\infty}dy\frac{y\exp(-z^2-y)}{(\beta+z)^2+y}, \quad (16)$$

where $\beta=B_z/\Delta B$ and ΔB is the dispersion of the nuclear hyperfine field distribution. ΔB is direction dependent for anisotropic electron g-tensor g_e, and can be expressed by [6]

$$\Delta B \propto \frac{\sqrt{\sum_j (A^j)^2}}{\mu_B g_e}, \quad (17)$$

where A is the hyperfine coupling constant and μ_B is the Bohr magneton. Figure 5(c) shows the magnetic field dependence of $R_\parallel(\infty)$ according to Eq. (16). Increasing β makes $R_\parallel(\infty)$ increase from 1/3 to 1. The suppression magnetic field $B_{\rm s}$ is defined when the spin polarization equals 90% of the difference between zero and strong β, $B_{\rm s}=3.8\Delta B$, as shown in Fig. 5(c). From the experimental data as shown in Figs. 5(a) and 5(b), the values of the suppression magnetic fields for the 90% points are 3.7 and 15.3 mT for the $4f(1)$ and $5d(1)$ states, respectively. Therefore, we can estimate $\Delta B_{[111]}=3.7/3.8\approx 1.0$ mT and $\Delta B_{[111]}=15.3/3.8\approx 4.0$ mT for the $4f(1)$ and $5d(1)$ states, respectively. In view of the fact that $g_{e[111]}$ equals 2.2 and 2.0 for the $4f(1)$ and $5d(1)$ electrons, respectively, the large difference of the ΔB values for the $4f(1)$ and $5d(1)$ states mainly comes from the difference of the hyperfine coupling strength between these two states as defined in Eq. (17). $\sqrt{\sum_j (A^j)^2}$ for the $4f(1)$ electrons is

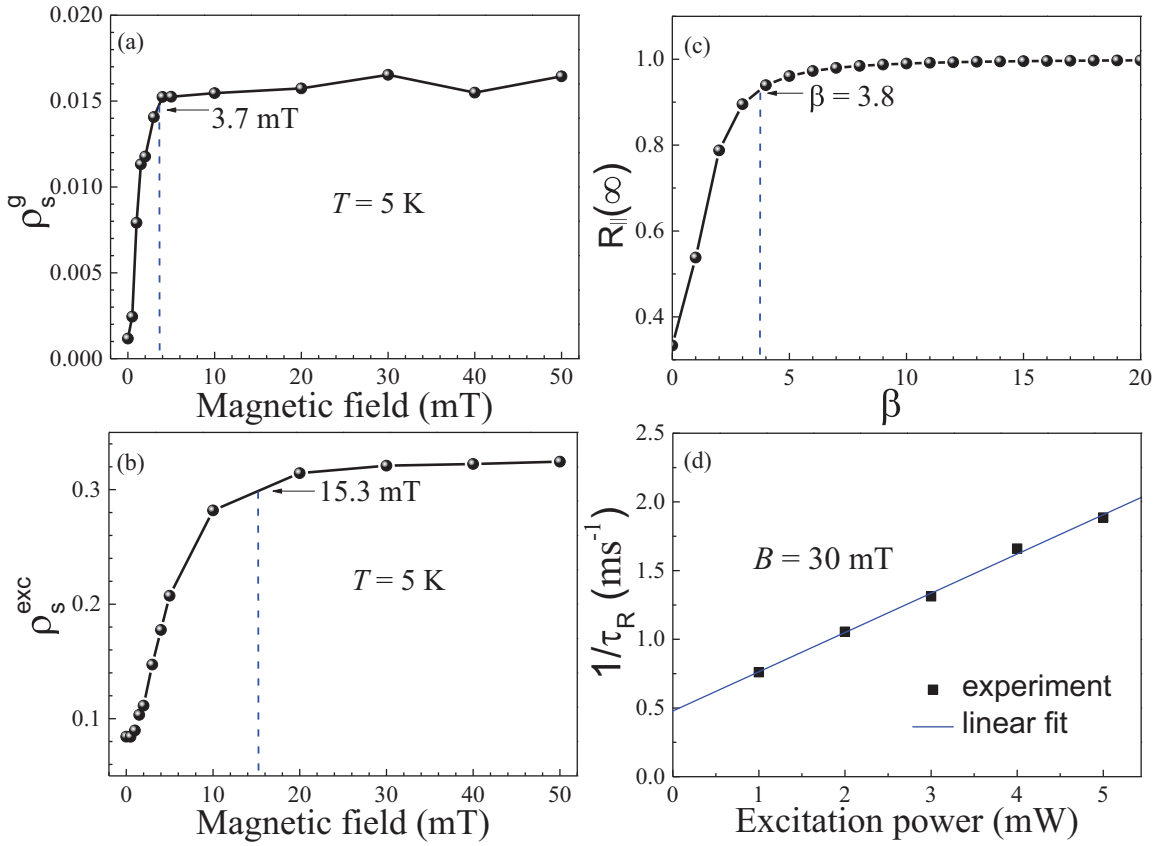

FIG. 5. External magnetic field dependence of the electron spin polarization of the Ce^{3+} ion in YAG crystals ($T = 5$ K). (a) ρ_s^g : the electron spin polarization of the $4f(1)$ state. (b) ρ_s^{exc} : the electron spin polarization of the $5d(1)$ state. (c) Calculated magnetic field dependence of $R_\parallel(\infty)$ according to Eq. (16) for an ensemble electron spin polarization that is instantaneously created. (d) Excitation power dependence of relaxation rates $1/\tau_R$ at $B = 30$ mT.

~4 times weaker than that for the $5d(1)$ electrons, which is comprehensible since the inner-shell $4f$ electrons of the Ce^{3+} ions have a more vanished Bloch function at the neighboring aluminum compared with the outer-shell $5d$ electrons. Note that the nuclear spin of almost all cerium and oxygen isotopes is 0, and the hyperfine influence of yttrium nuclear spin can be neglected [15]. The substitution of Ce^{3+} for Y^{3+} in the YAG crystal lattice forms a center electron spin. The neighboring Al^{3+} ions occupy either octahedral (2/5 ions) or tetrahedral (3/5 ions) sites [20,23]. The transferred hyperfine interaction with aluminum nuclei are expected from the Al^{3+} ions at the tetrahedral sites, which has been demonstrated by ENDOR spectra [19]. The ΔB value of 4 mT for the $5d(1)$ state is the same as that previously reported in Ref. [24] evaluated from laser-induced magnetization dynamics measurements. From the anisotropic $4f(1)$ electrons g tensor, $g_{[001]} = 2.738$, $g_{[110]} = 1.872$, $g_{[1\bar{1}0]} = 0.91$ [11], the dispersion of the local hyperfine field distribution for the three basic crystal directions can be deduced, with $\Delta B_{[001]} = 0.8$ mT, $\Delta B_{[110]} = 1.1$ mT, $\Delta B_{[1\bar{1}0]} = 2.4$ mT.

This spin lifetime defined by hyperfine interaction is on a timescale of 10 ns [16], below our experimental resolution. For a longitudinal magnetic field much larger than the suppression magnetic field B_s, the electron spin polarization of the $4f(1)$ state decays with the longitudinal lifetime T_1. According to Eq. (12), the spin relaxation rate $1/\tau_R$ is proportional to the excitation rate, and $1/T_1$ is thus equal to $1/\tau_R$ without the laser excitation. Figure 5(d) shows $1/\tau_R$ as a function of the excitation power. From the linear fit, we obtain τ_R at zero excitation, i.e., the longitudinal spin lifetime T_1, which equals 2.1 ms. This value at 5 K is comparable to 4.5 ms measured at 3.5 K for a single Ce^{3+} ion in YAG crystals [15]. The longitudinal spin lifetime T_1 for the $4f(1)$ state is defined by the spin-lattice relaxation time.

In principle, hyperfine interaction and continuous flip flops between electron and nuclear spins can lead to dynamical nuclear polarization (DNP), which can be verified by changing the modulation rate of the circularly polarized laser excitation [21,22]. In our experiments, the DNP effect does not show up, which is probably due to the fast relaxation rate of the environmental ^{27}Al nuclear 5/2 spin. Note that the ^{27}Al nuclear spin has not only dipole-dipole interactions, but also strong quadrupole interactions [19,20,23].

IV. CONCLUSION

In summary, we have investigated the electron spin dynamics of Ce^{3+} ions in YAG crystals at 5 K using time-resolved PL spectroscopy. By an alternating σ^+ and σ^- circularly polarized continuous-wave laser modulation technique, the electron spin polarization is periodically switched between spin-up and spin-down in accord with

the laser modulation rate. By solving the rate equations for the electron excitation and decay processes, electron spin polarization is quantitatively correlated to the PL signals. The spin signals of the $4f$ and $5d$ electrons can be well separated by analyzing the dynamics and steady-state circular polarization of PL transients. A longitudinal magnetic field can effectively suppress the electron spin relaxation due to hyperfine interaction between the electron spins both in the $4f$ and $5d$ states of Ce^{3+} ions and environmental nuclear spins. The suppression magnetic fields for the $4f$ electrons are four times weaker than that for the $5d$ electrons. After suppressing the hyperfine-induced spin relaxation, the electron spin polarization is increased by 16 times for the $4f$ electrons and four times for the $5d$ electrons. The spin-lattice relaxation time for the $4f$ electrons is 2.1 ms at 5 K. For the $5d$ electrons with isotropic g tensor, the dispersion of the nuclear hyperfine field distribution ΔB is 4.0 mT and direction independent. For the $4f$ electrons with anisotropic g tensor, $\Delta B_{[001]} = 0.8$ mT, $\Delta B_{[110]} = 1.1$ mT, $\Delta B_{[1\bar{1}0]} = 2.4$ mT. It reveals that the $4f$ electrons have ~4 times weaker hyperfine coupling strength than the $5d$ electrons.

ACKNOWLEDGMENTS

The authors are thankful to K. W. Xia for valuable discussions. This work was partially supported by the National Key Research and Development Program of China (Grants No. 2018YFA0306303 and No. 2016YFB0501601), the National Natural Science Foundation of China (Grants No. 11374099, No. 11474097, No. 11727810, No. 61720106009, and No. 11474096), the Shanghai Municipal Science and Technology Commission of China (Grant No. 16520721200), and the 111 Project of China (Grant No. B12024).

[1] D. Loss and D. P. DiVincenzo, Phys. Rev. A **57**, 120 (1998).
[2] A. Imamoğlu, D. D. Awschalom, G. Burkard, D. P. DiVincenzo, D. Loss, M. Sherwin, and A. Small, Phys. Rev. Lett. **83**, 4204 (1999).
[3] E. A. Zhukov, E. Kirstein, N. E. Kopteva, F. Heisterkamp, I. A. Yugova, V. L. Korenev, D. R. Yakovlev, A. Pawlis, M. Bayer, and A. Greilich, Nat. Commun. **9**, 1941 (2018).
[4] W. B. Gao, A. Imamoglu, H. Bernien, and R. Hanson, Nat. Photon. **9**, 363 (2015).
[5] D. H. Feng, X. Li, T. Q. Jia, X. Q. Pan, Z. R. Sun, and Z. Z. Xu, Appl. Phys. Lett. **100**, 122406 (2012).
[6] I. A. Merkulov, A. L. Efros, and M. Rosen, Phys. Rev. B **65**, 205309 (2002).
[7] A. Khaetskii, D. Loss, and L. Glazman, Phys. Rev. B **67**, 195329 (2003).
[8] A. V. Khaetskii, D. Loss, and L. Glazman, Phys. Rev. Lett. **88**, 186802 (2002).
[9] P.-F. Braun, X. Marie, L. Lombez, B. Urbaszek, T. Amand, P. Renucci, V. K. Kalevich, K. V. Kavokin, O. Krebs, P. Voisin, and Y. Masumoto, Phys. Rev. Lett. **94**, 116601 (2005).
[10] V. V. Belykh, D. R. Yakovlev, J. J. Schindler, E. A. Zhukov, M. A. Semina, M. Yacob, J. P. Reithmaier, M. Benyoucef, and M. Bayer, Phys. Rev. B **93**, 125302 (2016).
[11] H. R. Lewis, J. Appl. Phys. **37**, 739 (1966).
[12] M. Moszyński, T. Ludziejewski, D. Wolski, W. Klamra, and L. O. Norlin, Nucl. Instrum. Methods Phys. Res. A **345**, 461 (1994).
[13] M. Nikl, Meas. Sci. Technol. **17**, R37 (2006).
[14] R. Kolesov, K. Xia, R. Reuter, M. Jamali, R. Stöhr, T. Inal, P. Siyushev, and J. Wrachtrup, Phys. Rev. Lett. **111**, 120502 (2013).
[15] P. Siyushev, K. Xia, R. Reuter, M. Jamali, N. Zhao, N. Yang, C. Duan, N. Kukharchyk, A. D. Wieck, R. Kolesov, and J. Wrachtrup, Nat. Commun. **5**, 3895 (2014).
[16] D. V. Azamat, V. V. Belykh, D. R. Yakovlev, F. Fobbe, D. H. Feng, E. Evers, L. Jastrabik, A. Dejneka, and M. Bayer, Phys. Rev. B **96**, 075160 (2017).
[17] P. Liang, R. R. Hu, C. Chen, V. V. Belykh, T. Q. Jia, Z. R. Sun, D. H. Feng, D. R. Yakovlev, and M. Bayer, Appl. Phys. Lett. **110**, 222405 (2017).
[18] G. R. Asatryan, D. D. Kramushchenko, Yu. A. Uspenskaya, P. G. Baranov, and A. G. Petrosyan, Phys. Solid State **56**, 1150 (2014).
[19] D. V. Azamat, A. G. Badalyan, D. H. Feng, J. Lančok, L. Jastrabik, A. Dejneka, P. G. Baranov, D. R. Yakovlev, and M. Bayer, J. Appl. Phys. **122**, 243903 (2017).
[20] A. G. Badalyan, G. V. Mamin, Yu. A. Uspenskaya, E. V. Edinach, H. R. Asatryan, N. G. Romanov, S. B. Orlinskii, P. G. Baranov, V. M. Khanin, H. Wieczorek, and C. Ronda, Phys. Status Solidi B **254**, 1600631 (2017).
[21] I. A. Akimov, D. H. Feng, and F. Henneberger, Phys. Rev. Lett. **97**, 056602 (2006).
[22] D. H. Feng, I. A. Akimov, and F. Henneberger, Phys. Rev. Lett. **99**, 036604 (2007).
[23] Yu. A. Uspenskaya, G. V. Mamin, R. A. Babunts, A. G. Badalyan, E. V. Edinach, H. R. Asatryan, N. G. Romanov, S. B. Orlinskii, V. M. Khanin, H. Wieczorek, C. Ronda, and P. G. Baranov, AIP Adv. **8**, 035001 (2018).
[24] R. Kolesov, Phys. Rev. A **76**, 043831 (2007).